8. D. B. Graves, *J. Appl. Phys.*, **62,** 88 (1987).
9. J. P. Boeuf, *Phys. Rev. A.*, **36,** 2782 (1987).
10. J. H. Tsai and C. Wu, *ibid.*, **41,** 5626 (1990).
11. M. J. Kushner, *IEEE Trans. Plasma Sci.*, **PS-14,** 188 (1986).
12. T. A. Cleland and D. W. Hess, *This Journal*, **136,** 3103 (1989).
13. M. Dalvie, K. F. Jensen, and D. B. Graves, *Chem. Eng. Sci.*, **41,** 653 (1986).
14. M. Dalvie and K. F. Jensen, *J. Vac. Sci. Technol.*, **A8,** 1648 (1990).
15. J. A. Folta and R. C. Alkire, *This Journal*, **137,** 3173 (1990).
16. A. S. Kao, and H. G. Stenger, Jr., *ibid.*, **137,** 954 (1990).
17. J. Kobayashi, N. Nakazato, and K. Kiratsuka, *ibid.*, **136,** 1781 (1989).
18. S. P. Venkatesan, I. Trachtenberg, and T. F. Edgar, *ibid.*, **137,** 2280 (1990).
19. J. Liu, L. Huppert, and H. H. Sawin, *J. Appl. Phys.*, **68,** 3916 (1990).
20. D. J. Economou, D. R. Evans, and R. C. Alkire, *This Journal*, **135,** 756 (1988).
21. L. Kline and M. J. Kushner, *Critical Reviews in Solid State and Materials Sciences*, **16,** 1 (1989).
22. D. B. Graves, *AIChE J.*, **35,** 1 (1989).
23. D. J. Economou and R. C. Alkire, *This Journal*, **135,** 2786 (1988).
24. D. J. Economou, S. K. Park, and G. D. Williams, *ibid.*, **136,** 188 (1989).
25. J. Ignacio Ulacio F. and J. P. McVittie, in "Plasma Processing" G. S. Mathad, G. C. Schwartz, and D. W. Hess, Editors, PV 88-22, p. 43, The Electrochemical Society Softbound Proceedings Series, Pennington, NJ (1988).
26. G. L. Rogoff, J. M. Kramer, and R. B. Piejak, *IEEE Trans. Plasma Sci.*, **PS-14,** 103 (1986).
27. V. M. Donnelly, D. L. Flamm, and G. Collins, *J. Vac. Sci. Technol.*, **21,** 817 (1982).
28. V. M. Donnelly, D. L. Flamm, and R. Bruce, *J. Appl. Phys.*, **58,** 2135 (1985).
29. A. D. Richards, B. E. Thompson, K. D. Allen, and H. H. Sawin, *ibid.*, **62,** 792 (1987).
30. G. S. Selwyn, L. D. Baston, and H. H. Sawin, *Appl. Phys. Lett.*, **51,** 898 (1987).
31. E. S. Aydil and D. J. Economou, *This Journal*, **139,** 1406 (1992).
32. B. E. Cherrington, "Gaseous Electronics and Gas Lasers," Pergamon Press, New York (1979).
33. M. V. Kurepa, and D. S. Belic, *J. Phys. B*, **11,** 3719 (1978).
34. P. S. Ganas, *J. Appl. Phys.*, **63,** 277 (1988).
35. W. L. Morgan, Joint Inst. for Lab. Astrophysics, Univ. of Colorado, Boulder, Rep. 19 (1979).
36. D. L. Flamm and V. M. Donnelly, *J. Appl. Phys.*, **59,** 1052 (1986).
37. D. L. Flamm, *J. Vac. Sci. Technol.*, **A4,** 729 (1986).
38. S. K. Park and D. J. Economou, *J. Appl. Phys.*, **68,** 3904 (1990).
39. G. L. Rogoff, *J. Phys. D: Appl. Phys.*, **18,** 1533 (1985).
40. R. H. Perry and C. C. Chilton, "Chemical Engineers' Handbook," Fifth Edition, p. 3-247, McGraw-Hill, New York (1973).
41. A. C. Lloyd, *Int. J. of Chemical Kinetics*, Vol. III, 39 (1971).
42. E. A. Ogryzlo, *Can. J. Chem.*, **39,** 2556 (1961).
43. M. A. A. Clyne, and D. H. Stedman, *Int. J. of Chemical Kinetics*, **39,** 2698 (1971).
44. F. Kaufman, "Chemical Reactions in Electrical Discharges," Vol. 80, American Chemical Society (1969).
45. E. S. Aydil, Ph.D. Thesis, University of Houston, 1991.
46. A. T. Bell, in "Techniques and Applications of Plasma Chemistry," J. R. Hollahan, and A. T. Bell, Editors, p. 1, John Wiley & Sons, Inc., New York (1974).

Theoretical and Experimental Investigations of Chlorine RF Glow Discharges

II. Experimental

Eray S. Aydil[1] and Demetre J. Economou

Department of Chemical Engineering, University of Houston, Houston, Texas 77204-4792

ABSTRACT

Key plasma properties of a 13.56 MHz chlorine glow discharge were measured using several plasma diagnostic techniques. Electron density and energy, self-sustained electric field, RF current flowing through the plasma, ion bombardment energy, and atomic chlorine concentration were measured as a function of reactor operating conditions. The experimental data were compared to the predictions of a plasma reactor model which included details of the bulk plasma. Good agreement between the measured and predicted values of all the above plasma properties was obtained over a range of pressure, power, and electrode spacing without adjusting any reaction rate coefficients.

In the preceding paper (hereafter to be referred to as Part I), a comprehensive plasma reactor model for a chlorine discharge was developed including details of the bulk plasma (1). The model was used to predict key internal properties of the plasma such as the electron energy distribution function, electron density, self-sustained electric field, peak RF current, ion bombardment energy, and atomic chlorine concentration profiles. These internal plasma properties directly affect the plasma etching process outcome, namely, the etch rate, uniformity, and anisotropy. In order to test the model predictions, measurement of the key internal plasma properties is necessary.

Recent advances in *in situ* plasma diagnostic techniques have contributed to basic understanding of the plasma etching process (2). Optical emission spectroscopy and laser induced fluorescence (3-6), Langmuir probe measurements (7-9), mass spectrometry (10, 11), ion bombardment flux and energy analysis (12, 13), plasma impedance analysis (14, 15), and laser interferometry (16) have all proven most useful. Each of the above plasma diagnostic techniques has its own advantages and limitations. Thus, more than one diagnostic needs to be used to obtain complementary information. In this study, a variety of plasma diagnostics were used to monitor *in situ* key internal plasma properties, and to relate observed reactor performance to changes in easily controllable and measurable external variables such as power, pressure, flow rate, and reactor geometry.

There are a number of experimental studies of the chlorine plasma. Richards *et al.* (17) measured the atomic chlorine concentration in a parallel plate reactor using optical emission actinometry and infrared absorption spectroscopy. The authors found that the atomic chlorine mole fraction varied between 0 and 0.1. Rogoff *et al.* (18) inferred the atomic chlorine concentration in a similar-type reactor

[1] Present address: AT&T Bell Laboratories, Murray Hill, NJ 07974-2070.

from measurements of the molecular chlorine density using laser absorption. They reported that the atomic chlorine mole fraction varied between 0.4 and 0.6. Donnelly *et al.* (19) used laser induced fluorescence to measure the density of molecular chlorine ions in a chlorine discharge. Other investigators studied the negative ion density (20). Donnelly *et al.* (5), Flamm and Donnelly (21), and Flamm (22) studied the optical emission, electrical, and etching characteristics of the chlorine plasma, with emphasis on the effects of frequency. Bruce and Reinberg (23) studied the effect of dc bias on the ion bombardment energy distribution and on the etch profiles.

The information and insight gained from the above and other works were used in Part I to construct a comprehensive plasma reactor model of the chlorine discharge. In this paper, the model predictions are compared with experimental measurements in an empty reactor (no wafer present) in order to demonstrate the validity of the model.

Experimental System

The plasma reactor used in this study consisted of three chambers: an etching chamber, a sampling chamber, and a load lock-chamber. The reactor design is similar to that of Allen *et al.* (14). The etching chamber and the sampling chamber are shown in Fig. 1. The plasma was sustained between two equal-area, 20.3 cm diam parallel plate electrodes in the etching chamber. The spacing between the hard anodized aluminum showerhead upper electrode and stainless steel grounded lower electrode was adjustable and varied between 1.27 and 5 cm in this study. The lower electrode could be replaced by a hard anodized aluminum electrode to study the effects of different electrode material. The upper powered electrode was surrounded by a 5.08 cm wide Teflon ring, and the lower electrode was surrounded by a 7.62 cm wide floating alumina shield to aid in plasma confinement. The temperature of both electrodes was controlled by a chiller/heater (Bay Voltex, Tempryte, HS-3500-WC-DC-SX). The chamber pressure was controlled by a closed-loop system consisting of a pressure transducer (MKS 222B), an exhaust throttle valve (MKS 253), and a controller (MKS 252A). Gas flow rate was regulated by mass flow controllers (Unit Instruments UFC-1100). Gases used were ultra pure chlorine, and prepurified argon, the latter used for actinometry. The total gas flow rate was set at 25 sccm unless noted otherwise. The etching chamber was pumped by a two-stage rotary vane mechanical pump (Edwards E2M40) with Fomblin oil service and an external oil filtration unit. A 600 l/s diffusion pump with a LN_2 trap (Edwards Diffstak CR160) was used to remove residual water vapor and achieve a background pressure of less than 10^{-5} Torr. Power was applied to the upper showerhead electrode by a 500 W, 13.56 MHz generator (RF Plasma Products RF5S) and was coupled to the plasma through an impedance matching network. The forward and reflected power were monitored by a directional wattmeter (Bird 4410A). The applied power was very stable and the reflected power was typically less than 0.5% of the forward power. The actual power dissipated in the discharge was measured with a digitizing oscilloscope (see below).

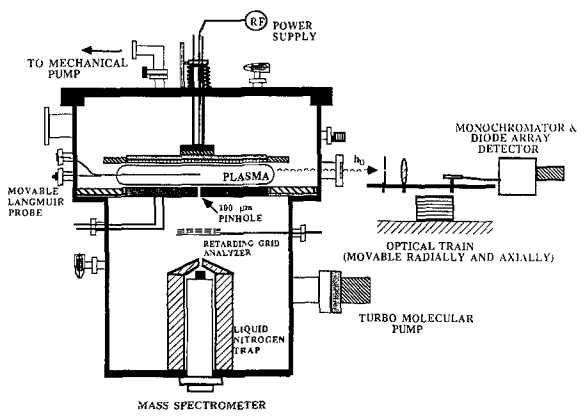

Fig. 1. Schematic of the experimental system and plasma diagnostics.

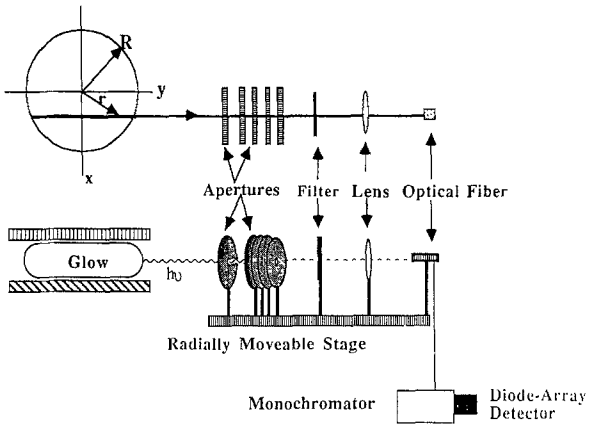

Fig. 2. Spatially resolved optical emission collection system.

The sampling chamber was differentially pumped with a 50 l/s turbomolecular pump (Balzers TPU050) and could communicate with the etching chamber through a 100 μm diam pinhole on the lower electrode. Plasma species incident onto the lower electrode were sampled through this pinhole and analyzed with a mass spectrometer (UTI 100C with HP data acquisition) situated directly under the pinhole. The mass spectrometer was encased in a liquid nitrogen trap to lower the background pressure of condensible gases. The base pressure in the lower chamber was typically less than 10^{-6} Torr. A retarding grid energy analyzer/Faraday cup assembly placed between the pinhole and the mass spectrometer (Fig. 1) was used to measure the ion bombardment flux and energy distribution function (12, 13).

The optical emission collection system (Fig. 2) was similar to the one described by Economou *et al.* (24). Plasma emission was collected through a quartz side window, and passed through five iris diaphragms in order to attain spatial resolution and reduce reflections. A filter was used to block plasma emission at wavelengths less than 500 nm in order to avoid second-order interference in the spectrum. The light was focused onto the end of an optical fiber with the aid of a lens, and was transmitted to the entrance slit of a monochromator (Thermo Jarrell Ash Monospec 27). A diode-array detector (Princeton Instruments RY-1024 with ST-120 controller and PC data acquisition) was used to detect and record spectra. The optical train was mounted on a movable stage which could be translated on a plane parallel to the electrodes by a stepping motor. Thus, spectra were obtained as a function of the side-on observation coordinate. The data were processed using principles of optical emission actinometry (3) and the Abel transformation (24) to obtain the radial emission and in turn the concentration profiles of atomic chlorine.

Application of actinometry to monitor the atomic chlorine concentration in a chlorine discharge requires care. Actinometry can be used when the excited state whose emission is being monitored is created only by electron impact excitation from the ground state. The contribution to production of excited atomic chlorine of other pathways, such as dissociative excitation and dissociative attachment must be negligible. Gottscho and Donnelly (4) concluded from observations of the spectral line shapes that actinometry is invalid for Cl atoms if the emission from the sheaths is sampled. However, the authors found that actinometry can be used to monitor atomic chlorine concentration if emission is sampled from the plasma center, excluding the sheaths. Richards *et al.* (17) found actinometry to be invalid for monitoring Cl atoms in a chlorine discharge. However, the authors sampled plasma emission from the entire discharge, including the sheaths. Flamm and Donnelly (21) concluded that actinometry can give an erroneous measure of atom concentration if the viewing area is not restricted to the center of the plasma. In the present study, care was taken to sample emission from the

central plane of the discharge, away from the sheaths. A small amount (5% by volume) of argon was added as the actinometer gas. Either the 837.6 nm or the 808.7 nm Cl line was monitored, along with 811.5 nm Ar actinometer line. When using the 808.7 nm line, the dependence of Cl concentration on pressure and power was nearly identical to the laser absorption measurements of Richards *et al.* (17). Hence the 808.7 nm, line was preferred over the 837.6 nm line.

The Faraday cup/ion grid analyzer was similar to the one used by other investigators who have also described the principles of operation (11-13, 25). Briefly, the analyzer consisted of three high-transmission tungsten grids and a stainless steel plate which served as a Faraday cup. The energy distribution of ions bombarding the electrode was determined by applying a constant negative potential to the top grid in order to repel electrons, and measuring the current I_+ at the Faraday cup as a function of the positive potential V_a applied to the center grid. The ion energy distribution function was calculated from the Faraday cup current-voltage characteristics using

$$f_{IED}(E_+) = -\frac{1}{I_{+0}}\frac{dI_+(E_+)}{dE_+} \quad [1]$$

where $E_+ = eV_a$. The total ion current, I_{+0}, through the pinhole was measured using a picoammeter (Keithley 619) by biasing all grids and the cup at a large negative potential (−50 to −100 V). The total ion current was the sum of the currents collected by the grids and the Faraday cup. The mean ion energy was calculated from the distribution function. The mean energy is defined by

$$\bar{E}_+ = \int_0^\infty E_+ f_{IED}(E_+)dE_+ \quad [2]$$

The median energy is defined such that the fraction of ions having energies below or above the median energy is 0.5. Assuming that the ions are singly charged, the median energy corresponds to the potential V_a at which the Faraday cup current is equal to $I_{+0}/2$. The median energy can be measured very conveniently without recording the entire ion energy distribution function. The ratio of mean to median ion energy was found to be approximately constant.

Several types of Langmuir probes were used in this study, including a double asymmetric Langmuir probe, a single probe operating in the orbital motion limited (OML) regime, and a single probe operating in the thin sheath limit regime. The double asymmetric probe consisted of two tungsten wires encaged by a 0.635 cm od ceramic tube. The larger wire had a diam of 0.1 cm and protruded 1 cm from the tip of the ceramic holder. The smaller wire was 0.0127 cm in diam and protruded 0.25 cm from the tip of the ceramic holder. The two wires were separated by 0.1 cm. The larger wire was also used independently as a single probe operating in the thin sheath limit regime, and the smaller wire was used as a single probe operating in the OML regime. An RF filter consisting of a network of inductors and capacitors was used to minimize the RF current collected by the probes. The literature on the Langmuir probes is voluminous. References (27-31) are particularly thorough reviews.

The current and voltage waveforms were measured at the RF feedthrough and corrected for stray capacitance (165 pF, in parallel with the plasma impedance) and line inductance (0.5 μH, in series with the plasma). The stray capacitance and line inductance were measured using standard techniques (12, 32) as well as from the network resonance frequency for different electrode spacings in the absence of a plasma. Different methods agreed to within 5%. The current was measured using a wide band current transformer (Pearson Model 4100), and the voltage was sampled through a high voltage probe (Tektronix P6134). Both current and voltage waveforms were recorded using a 500 MHz digitizing oscilloscope (Textronix 11401). The actual power dissipated in the plasma was calculated from the product of the corrected current and voltage waveforms, accounting for the phase shift. The power was found to be greater than 90% of the nominal power for most cases (see Results and Discussion)

Impedance Analysis

Measurement of the current and voltage waveforms can provide considerable information about the internal plasma properties if an appropriate equivalent circuit of the discharge can be constructed. Allen *et al.* (14), Zarowin (15), Butterbaugh *et al.* (33), and Ulacia and McVittie (34) have demonstrated the utility of this technique. In the present study, impedance analysis was used to estimate some important plasma properties, such as electron density, time-average sheath capacitance, thickness, and voltage as well as the bulk plasma resistance.

Using the model described in Part I, it was established that for the parameter range of interest the chlorine bulk plasma acts as a resistor R_p. In addition, the power dissipated in the sheaths as estimated from the measured ion bombardment flux and sheath voltage was a small fraction of the total power input. Hence the sheaths may be represented as ideal capacitors with capacitance C_S. Under these conditions the equivalent circuit of Zarowin (15) reduces to the circuit shown in Fig. 3, which was used for the impedance analysis in this study. The same simplified equivalent circuit has been used before by other investigators (14, 35). The plasma resistance and sheath capacitance can be calculated from the measured current and voltage waveforms and the phase shift ϕ between the two using

$$R_p = \frac{V_0}{I_0}\cos\phi \quad [3]$$

$$C_s = \frac{I_0}{\pi\upsilon_a V_0 \sin\phi} \quad [4]$$

The average electron density, $<n_e>$, time-averaged sheath potential, V_S, and time-averaged sheath thickness, d_S, can be calculated from

$$<n_c> = \frac{2L}{eA\mu_e R_p} \quad [5]$$

$$V_S = \frac{I_0}{2\pi\upsilon_a C_S} \quad [6]$$

$$d_S = \epsilon_0\frac{A}{C_S} \quad [7]$$

In addition one can calculate the effective self-sustained bulk electric field to neutral density ratio (E/N) from

$$\frac{E}{N} = \frac{V_0\cos\phi}{2\sqrt{2}\,L} \quad [8]$$

The product of electron mobility and neutral gas density was taken to be constant at 5.633×10^{21} (cm-V-s)$^{-1}$.

Despite the care taken to confine the plasma between the electrodes, the plasma volume changed as power and pressure were varied. Expansion of the plasma by even 1 cm beyond the 10.15 cm electrode radius results in an increase of the plasma volume by 21%. In order to account

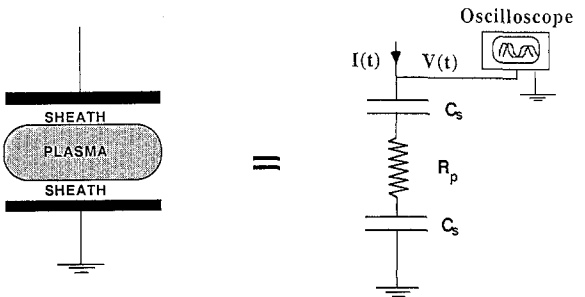

Fig. 3. Equivalent circuit for the chlorine plasma used in the impedance analysis.

for variations in the plasma volume, the plasma radius was measured as a function of operating conditions using spatially resolved optical emission. The plasma emission intensity was found to decrease gradually over a few cm beyond the electrode edge. In the following comparisons the measured plasma radius was used to calculate the plasma volume. All measurements reported below were performed in an empty reactor (no wafer present).

Results and Discussion

The power efficiency was defined as the ratio of power dissipated in the plasma (measured from the corrected voltage and current waveforms) to the nominal power (measured by a Bird power meter). The power efficiency decreased with increasing plasma impedance. It was greater than 90% when the total plasma impedance was less than about 200 Ω. The impedance of the chlorine plasma decreased with increasing power and decreasing pressure. The plasma impedance was less than 200 Ω when the pressure was below 0.5 Torr and at the same time the RF power was above 25 W. As pressure was increased, a higher power was required (>75 W at 1 Torr) to keep the plasma impedance below 200 Ω. The dependence of power efficiency on plasma impedance was studied recently by Godyak and Piejak (32). The power reported in all the figures below is that dissipated in the plasma.

The plasma impedance is the sum of the capacitive sheath impedance and the bulk plasma resistance. It was found that the sheaths contributed 20-50% to the total impedance, depending on operating conditions. As a result, the measured phase shift between voltage and current waveforms varied between 25° at low power and/or high pressure conditions (low electron density, high bulk resistance) to 70° at high power and/or low pressure conditions (high electron density, low bulk resistance). In contrast to SF_6, which is also strongly electronegative (36, 37), the chlorine discharge did not show any inductive behavior in the parameter range investigated in this study.

The bulk plasma model (see Part I) is capable of predicting the self-sustained electric field, time-averaged electron density, peak current flowing through the plasma, and electron impact reaction rate coefficients. Figure 4 shows a comparison between the predicted and measured rms self-sustained electric field to neutral density ratio as a function of $N\Lambda$. It was shown theoretically that the self-sustained field is a function of $N\Lambda$ only for a given atomic chlorine mole fraction (1). In Fig. 4 the $(E/N)_{rms}$ measured for a range of pressure (0.2-1 Torr), power (20-200 W), and electrode spacing (1.27-2.54 cm) is compared to the theoretical predictions (solid lines) calculated for an atomic chlorine mole fraction of 0 and 0.2. The atomic chlorine mole reaction was less than 0.2 as the pressure, power, and electrode spacing were varied. The accuracy of the impedance analysis used to determine $(E/N)_{rms}$ is similar to the difference between the theoretical curves for

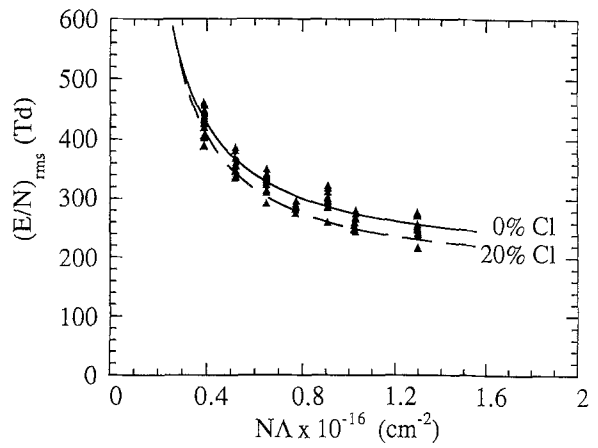

Fig. 4. Comparison of measured (points) and calculated (lines) root mean square self-sustained electric field to neutral density ratio as a function of $N\Lambda$.

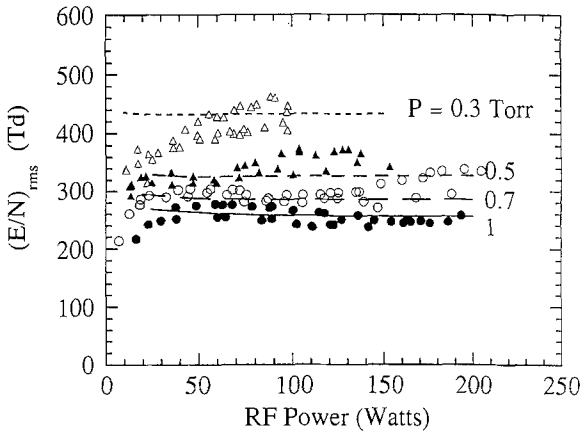

Fig. 5. Comparison of measured (points) and calculated (lines) root mean square self-sustained electric field to neutral density ratio as a function of RF power.

0 and 0.2 atomic chlorine mole fraction. The agreement between the predicted and measured E/N is satisfactory considering the fact that the bulk plasma model does not contain any adjustable parameters. The theory further predicted that, for moderate changes in the atomic chlorine mole fraction, the self-sustained electric field is a weak function of the RF power. The measured and calculated self-sustained electric field as a function of power is shown in Fig. 5, which confirms the model prediction. The disagreement between theory and experiment at low power is due to the high plasma impedance which introduces higher error in the measurement of E/N.

The electron density, measured by impedance analysis, is shown in Fig. 6 as a function of power for several pressures and for 1.27 cm electrode spacing. The agreement between theory and experiment is satisfactory considering that no adjustable parameters were used. The electron density increases linearly with power and decreases with pressure. At high power, the dependence turns into sublinear, because the plasma volume also increases. The decrease of electron density with pressure may be partly counterbalanced by the decrease of plasma volume as pressure increases. In fact, depending on the plasma confinement method used, changes in plasma volume may dominate the dependence of electron density on pressure. This underscores the need for physically or magnetically confining the plasma in commercial reactors to achieve high power density. This in turn results in high reactive radical concentration, ion bombardment energy, and etch rate. The measured and calculated electron density also agreed when the interelectrode spacing was 2.54 cm. The electron density decreased with increasing electrode spacing because of decrease in power density and increase in $N\Lambda$ (see Fig. 10 of Part I).

Predicted and measured values of the peak current, I_0, flowing through the plasma as a function of power and pressure for 1.27 cm electrode spacing are shown in Fig. 7. Good agreement between theory and experiment is again seen. The current increases with increasing power and decreases with increasing pressure because the electron density has the same dependence on power and pressure. Measured values of peak current as a function of power and pressure for an electrode spacing of 2.54 cm agreed equally well with the calculated values, in the absence of complicating phenomena, such as multiple steady-states (38). The peak current decreased with increasing electrode spacing because the average electron density decreased, and the current path increased causing the plasma resistance to increase. Hence, one may also think of the current decrease with increasing electrode spacing as being due to an increase in the bulk plasma resistance (for constant power). The current was sinusoidal for a 2.54 cm electrode spacing but became somewhat distorted as the electrode spacing was decreased below 1.5 cm. The current was assumed to be sinusoidal in the bulk plasma model. The agreement between theory and experiment even at

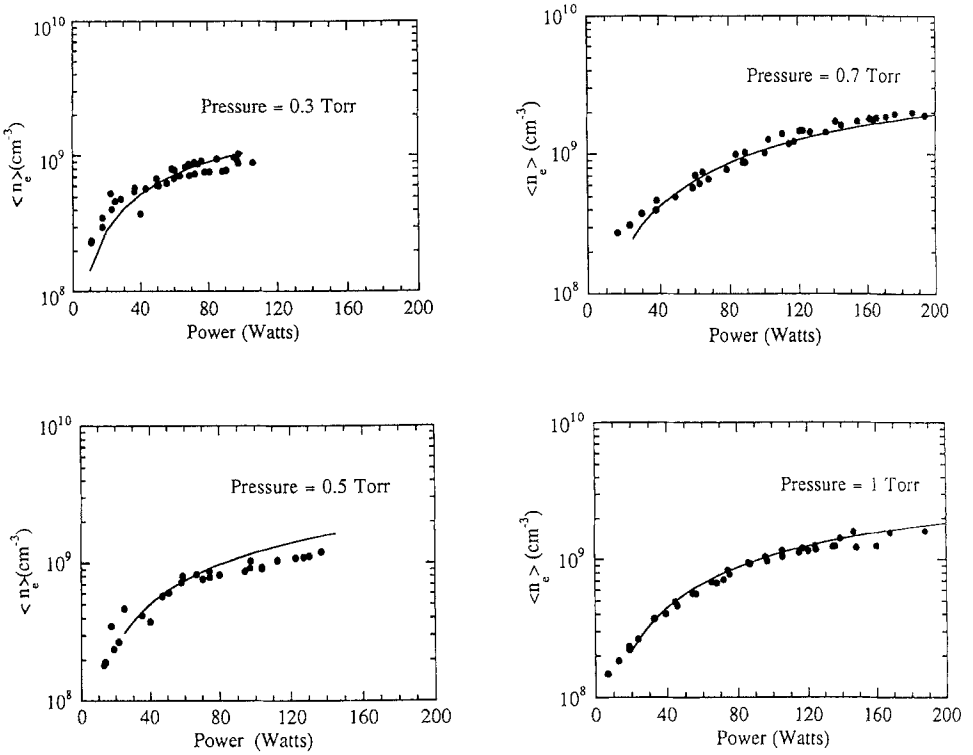

Fig. 6. Comparison of measured (points) and calculated (lines) time-averaged electron density as a function of RF power for 1.27 cm electrode spacing, 25 sccm, and (a) 0.3; (b) 0.5; (c) 0.7; and (d) 1.0 Torr.

1.27 cm electrode spacing indicates that the bulk plasma behavior is determined primarily by the fundamental frequency and that the effect of harmonics appears to be of secondary importance for the parameter range studied.

Double Langmuir probe theory was used to determine the electron "temperature" from the probe current-voltage characteristics (28). The probe theory assumes that the electron energy distribution function (EEDF) is Maxwellian. However, the EEDF for the chlorine plasma calculated using the Boltzmann transport equation was non-Maxwellian (see Part I). Nevertheless, the electron "temperature" calculated from the probe theory is indicative of the energy of the electrons. The measured electron temperature was 3.5 ± 0.5 eV at 0.4 Torr and 2.54 cm electrode spacing. For comparison, the calculated time-averaged characteristic energy was found to be 4.5 eV. The mean electron energy was calculated to be 3.3 eV (39). The radial uniformity of electron density was tested by measuring the double probe saturation current as a function of radial position in the central plane of the reactor. The saturation current was constant to within 10% from center to electrode edge, decreasing thereafter to zero at the edge of the plasma over a distance of a few cm. There were radial charge density and electron energy gradients at the edge of the plasma which penetrated into the plasma a distance approximately equal to the interelectrode gap.

The time-averaged sheath voltage calculated from Eq. [6] was used as input to the sheath model described in Part I to predict the mean ion bombardment energy (normal to the electrode) as a function of power, pressure, and electrode spacing. The collision cross section used for the Cl_2-Cl_2^+ system was 1.5×10^{-16} cm^2 close to 2.57×10^{-16} cm^2 reported in the literature (40). The predicted and measured values are compared in Fig. 8 for 1.27 cm interelectrode gap. Similar trends were obtained for an interelectrode spacing of 2.54 cm and for pressure less than 0.5 Torr (for which a plasmoid does not form). From the ion energy distribution functions measured at several conditions, it was found that the ratio of mean to median ion energy was constant. A number of the experimental data points of mean energy shown in Fig. 8 were obtained by measuring the median energy without measuring the complete distribution function. At low pressure ($P < 0.5$ Torr) the ion bombardment energy increases rapidly as a function of power primarily due to increasing sheath voltage. In addition, the

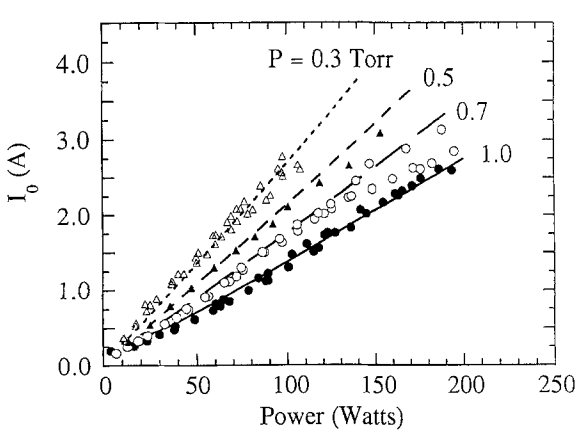

Fig. 7. Comparison of measured (points) and calculated (lines) peak current as a function of RF power. The interelectrode gap was 1.27 cm and the flow rate was 25 sccm.

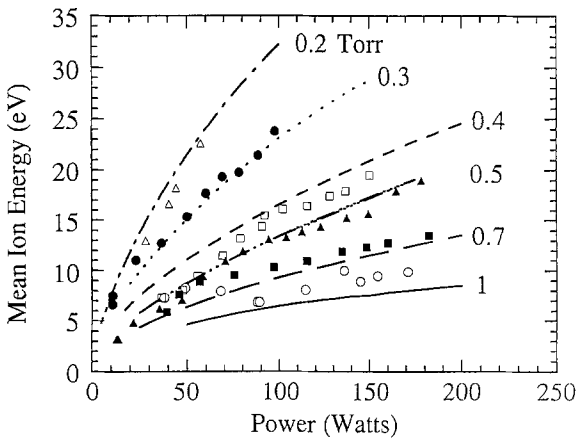

Fig. 8. Comparison of measured (points) and calculated (lines) mean ion bombardment energy as a function of RF power for several pressures. The interelectrode gap was 1.27 cm and the flow rate was 25 sccm.

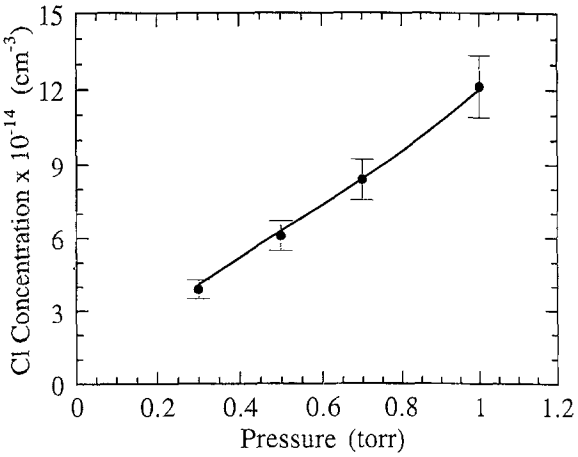

Fig. 9. Comparison of measured (points) and calculated (line) atomic chlorine concentration in the center of the reactor as a function of pressure. Other conditions were 1.27 cm interelectrode spacing, 25 sccm, and 100 W.

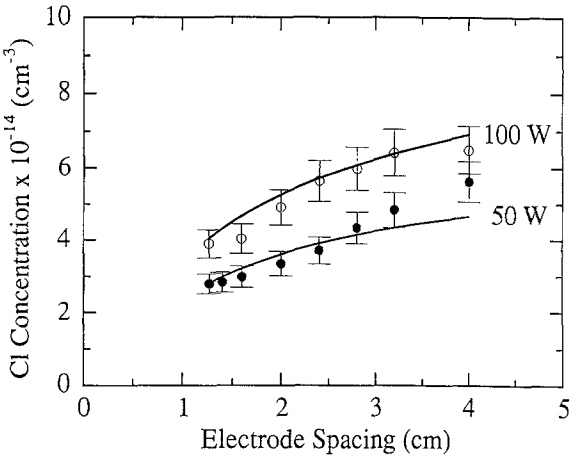

Fig. 10. Comparison of measured (points) and calculated (lines) atomic chlorine concentration in the center of the reactor as a function of interelectrode spacing. Other conditions were 0.5 Torr and 25 sccm.

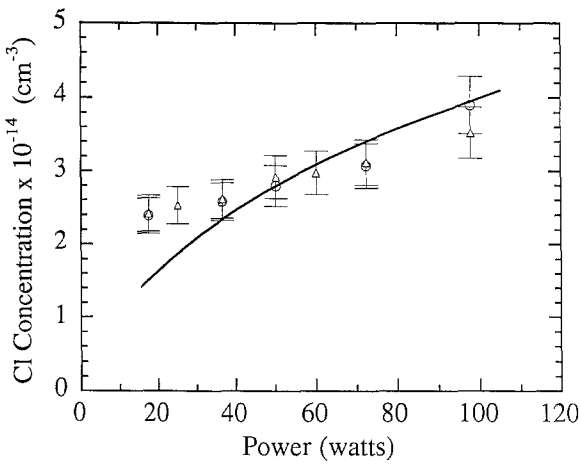

Fig. 11. Comparison of measured (points) and calculated (line) atomic chlorine concentration in the center of the reactor as a function of RF power. Other conditions were 0.3 Torr, 1.27 cm electrode spacing, and 25 sccm.

sheath thickness decreases with increasing power, and thus ions suffer fewer collisions in the sheath contributing to the increase in the mean ion bombardment energy. For example, at 0.3 Torr the sheath thickness decreased from 2.5 V at 25 W to 70 V at 100 W, while the sheath thickness decreased from 0.1 to 0.07 cm. Increasing pressure results in lower mean ion bombardment energy due to increasing number of collisions in the sheath. The mean ion bombardment energy seems to saturate as a function of power at high pressures. Both sheath voltage and thickness were found to be relatively weak functions of power at high pressures, causing this saturation in ion energy.

The mean ion bombardment energy was found to be only a fraction of the sheath voltage which implies that ions lose energy to collisions with neutrals. As pressure decreases, ions suffer fewer collisions in the sheath and the mean ion energy gets closer to the sheath voltage. The maximum energy observed in the ion energy distribution function was equal to the sheath voltage. Ions which possessed the maximum energy were those which had traversed the sheath without undergoing any collisions.

In the absence of etchable material and for sufficiently low values of flow rate and pressure, the dominant loss mechanism for atomic chlorine is recombination on the reactor walls. Experiments performed with an electrode made either of stainless steel or of aluminum covered by an anodization layer revealed that the atomic chlorine concentration did not depend on the choice of wall material. Figure 9 shows the atomic chlorine concentration at the reactor center (measured by actinometry) as a function of pressure. Each data point is the average of over 10 experiments performed on different days. The solid line is the calculated concentration using the second order surface recombination reaction rate coefficient reported by Allen for stainless steel (3.1×10^{-12} cm^4/s) (41). Since actinometry provides only relative concentrations, a least squares fit of the data was used to determine the proportionality constant between concentration and emission intensity (actinometric coefficient). The same constant was also used for Fig. 10 and 11 below.

Figure 10 shows that the atomic chlorine concentration increases with increasing spacing. The atom production rate varies as L^{-1} and the diffusion rate varies as L^{-2}. Hence, if diffusion is the dominant loss mechanism of atomic chlorine, the atom concentration should increase linearly with spacing (see also Fig. 14 of Part I). It is evident from Fig. 10 that diffusion limitations do play an important role, although the process is not totally diffusion controlled. The solid lines in Fig. 10 are theoretical predictions using the same values for surface recombination rate coefficient and actinometric coefficient as in Fig. 9.

The dependence of atomic chlorine concentration on power is shown in Fig. 11. Theoretically, the atomic chlorine concentration varies linearly with power for first order surface recombination kinetics, and as the square root of power for second order kinetics (1). The results of Fig. 9-11 demonstrate that the etchant transport and reaction model captures the dependence of atomic chlorine concentration on reactor operating conditions without adjusting any reaction rate coefficients.

Summary and Conclusions

Key plasma properties of a 13.56 MHz chlorine glow discharge were measured using several plasma diagnostic techniques. The plasma properties studied included the electron density and energy, self-sustained electric field, RF current flowing through the plasma, ion bombardment energy, and atomic chlorine concentration. The measurements were performed in a parallel plate single-wafer plasma reactor in the absence of a wafer (empty reactor). Plasma diagnostics included spatially resolved optical emission actinometry, single and double asymmetric Langmuir probe analysis, ion bombardment flux and energy analysis, and plasma impedance analysis.

The experimental data were compared to the predictions of a plasma reactor model. The model coupled the solution of the Boltzmann transport equation to a bulk plasma model to predict the electron density and energy, and the rate coefficients of electron impact reactions. These were in turn used in a species transport and reaction model to calculate the atomic chlorine concentration distribution in the reactor. Good agreement between the measured and predicted values of electron density and energy, self-sustained electric field, RF current flowing through the plasma, ion bombardment energy, and atomic chlorine concentra-

tion was obtained over a range of pressure, power, and electrode spacing without adjusting any reaction rate coefficients.

Experimental measurements under well-controlled conditions are essential for understanding the intricate phenomena occurring in reactive gas plasmas, and for testing mathematical models of plasma reactors. A combined experimental-modeling approach such as the one taken here is crucial for further refinement and extension of the mathematical models.

Acknowledgments

We are grateful to the National Science Foundation (CBT 8708908), Texas Instruments, the Welch Foundation, and the Texas Higher Education Coordinating Board (Texas Advanced Research Program) for financial support of this work. Thanks are also due to Dr. Gabe Barna, Dr. Lee Lowenstein, and Dr. Wayne Fisher of Texas Instruments for technical support and to Mr. Shashank Deshmukh for his help in the laboratory.

Manuscript submitted March 28, 1991; revised manuscript received Jan. 20, 1992.

The University of Houston assisted in meeting the publication costs of this article.

LIST OF SYMBOLS

A	electrode area, cm^2
C_S	time-averaged sheath capacitance, F
d_S	time-averaged sheath thickness, cm
E	electric field, V/cm
E_+	ion bombardment energy, eV
e	electronic charge, $1.609\ 10^{-19}$ C
f_{IED}	ion energy distribution function
I_0	peak RF current, A
$I_{+,0}, I_+$	ion bombardment flux, A
k_B	Boltzmann's constant, eV/K
L	half interelectrode gap, cm
N	total neutral density, cm^{-3}
n_e	electron density, cm^{-3}
P	pressure, Torr
R_p	bulk plasma resistance, Ω
V_0	peak RF voltage, V
V_a	voltage applied to the energy selector (center) grid of the ion energy analyzer, V
V_S	time-averaged sheath voltage, V

Greek symbols

ϵ_0	permittivity of free space, 8.8542×10^{-12} C^2/J-m
μ	mobility, cm^2/V-s
υ_a	applied excitation frequency, s^{-1}
ϕ	phase shift

Subscript

+	positive ions
e	electrons

Superscript

−	mean value

REFERENCES

1. E. S. Aydil and D. J. Economou, *This Journal*, **139,** 1396 (1992).
2. "Plasma diagnostics: Discharge Parameters and Chemistry," O. Auciello and D. L. Flamm, Editors, Academic Press Inc., New York (1989).
3. J. W. Coburn and M. Chen, *J. Appl. Phys.*, **51,** 3134 (1980).
4. R. A. Gottscho and V. M. Donnelly, *ibid.*, **56,** 245 (1984).
5. V. M. Donnelly, D. L. Flamm, and R. H. Bruce, *ibid.*, **58,** 2135 (1985).
6. R. A. Gottscho and T. A. Miller, *Pure and Appl. Chem.*, **56,** 189 (1984).
7. Ch. Steinbruchel, *This Journal*, **130,** 648 (1983).
8. T. I. Cox, V. G. I. Deshmukh, D. A. O. Hope, A. J. Hydes, N. St. J. Braithwaite, and N. M. P. Benjamin, *J. Phys. D: Appl. Phys.*, **20,** 820 (1987).
9. B. Lipschultz, I. Hutchinson, B. LaBombard, and A. Wan, *J. Vac. Sci. Technol.*, **A4,** 1810 (1986).
10. J. W. Coburn, *This Solid Films*, **171,** 65 (1989).
11. L. M. Ferreiro, D. W. Ernie, and J. F. Oskam, *J. Vac. Sci. and Technol.*, **A5,** 2280 (1987).
12. B. E. Thompson, K. D. Allen, A. D. Richards, and H. H. Sawin, *J. Appl. Phys.*, **53,** 2241 (1988).
13. W. M. Greene, M. A. Hartney, W. G. Oldham, and D. W. Hess, *ibid.*, **63,** 1367 (1988).
14. K. D. Allen, H. H. Sawin, M. T. Mocella, and M. W. Jenkins, *This Journal*, **133,** 2315 (1986).
15. C. B. Zarowin, *ibid.*, **130,** 1144 (1983).
16. H. Busta, R. E Lajos, and D. A. Kiewit, *Solid State Technol.*, **22,** 61 (1979).
17. A. D. Richards, B. E. Thompson, K. D. Allen, and H. H. Sawin, *J. Appl. Phys.*, **62,** 792 (1987).
18. G. L. Rogoff, J. M. Kramer, and R. B. Piejak, *IEEE Trans. Plasma Sci.*, **PS-14,** 103 (1986).
19. V. M. Donnelly, D. L. Flamm, and G. Collins, *J. Vac. Sci. Technol.*, **21,** 817 (1982).
20. J. Kramer, *J. Appl. Phys.* **60,** 3072 (1986).
21. D. L. Flamm and V. M. Donnelly, *ibid.*, **59,** 1052 (1986).
22. D. L. Flamm, *J. Vac. Sci. Technol.*, **A4,** 729 (1986).
23. R. H. Bruce and A. R. Reinberg, *This Journal*, **129,** 393 (1982).
24. D. J. Economou, S.-K. Park, and G. D. Williams, *ibid.*, **136,** 188 (1989).
25. K. D. Allen and H. H. Sawin, *ibid.*, **133,** 2326 (1986).
26. J. W. Coburn, *Rev. Sci. Instrum.*, **41,** 1219 (1970).
27. J. G. Laframboise, Institute for Aerospace Studies, Report No 100, Univ. of Toronto, 1966.
28. J. D. Swift and M. J. R. Schwar "Electrical Probes for Plasma Diagnostics," Elsevier New York (1969).
29. F. F. Chen in "Plasma Diagnostic Techniques," R. H. Huddlestone and S. L. Leonard, Editors, p. 113, Academic Press, New York (1965).
30. R. M. Clements, *J. Vac. Sci. Technol.*, **15,** 193 (1978).
31. H. Amemiya, *J. Phys. D: Appl. Phys.*, **23,** 999 (1990).
32. V. A. Godyak and R. B. Piejak, *J. Vac. Sci. Technol.*, **A8,** 3833 (1990).
33. J. W. Butterbaugh, L. D. Baston, and H. H. Sawin, *ibid.*, **A8,** 916 (1990).
34. J. I. Ulacia F. and J. P. McVittie, *MRS Symp Proc.*, **98** 203 (1987).
35. A. D. Richards and H. H. Sawin, *J. Appl. Phys.*, **62,** 799 (1987).
36. H. Shan, S. A. Self, and J. P. McVittie, Abstract 103, p. 145, Electrochemical Society Extended Abstracts, Vol. 90-1, Montreal, Quebec, Canada, May 6-11 (1990).
37. E. Gogolides, J-P Nicolai, and H. H. Sawin, *J. Vac. Sci. Technol.*, **A7,** 1001 (1989).
38. E. S. Aydil and D. J. Economou, *J. Appl. Phys.*, **69,** 109 (1991).
39. E. S. Aydil and D. J. Economou, in "Plasma Processing," G S. Mathad and D. W. Hess, Editors, *PV 90-14*, p. 77, The Electrochemical Society Softbound Proceedings Series, Pennington, NJ (1990).
40. E. W. McDaniel and E. A. Mason, "Mobility and Diffusion of Ions in Gases," J. Wiley and Sons Inc., New York (1973).
41. K. D. Allen, Ph.D. Dissertation, MIT (1986).
42. E. Gogolides and H. H. Sawin, *This Journal*, **136,** 1147 (1989).
43. A. D. Richards and H. H. Sawin, *J. Appl. Phys.*, **62,** 799 (1987).